J. Micromech. Microeng. **18** (2008) 055017 (7pp) doi:10.1088/0960-1317/18/5/055017

The design, fabrication and evaluation of a MEMS PZT cantilever with an integrated Si proof mass for vibration energy harvesting

Dongna Shen[1,2], Jung-Hyun Park[1,2], Jyoti Ajitsaria[2], Song-Yul Choe[2], Howard C Wikle III[1,2] and Dong-Joo Kim[1,2]

[1] Materials Research and Education Center, Auburn University, Auburn, AL 36849, USA
[2] Department of Mechanical Engineering, Auburn University, Auburn, AL 36849, USA

E-mail: Dongna.Shen@auburn.edu and dkim@eng.auburn.edu

Received 10 January 2008, in final form 20 February 2008
Published 4 April 2008
Online at stacks.iop.org/JMM/18/055017

Abstract
A microelectromechanical system (MEMS) piezoelectric energy harvesting device, a unimorph PZT cantilever with an integrated Si proof mass, was designed for low vibration frequency and high vibration amplitude environment. Pt/PZT/Pt/Ti/SiO_2 multilayered films were deposited on a Si substrate and then the cantilever was patterned and released by inductively coupled plasma reactive ion etching. The fabricated device, with a beam dimension of about 4.800 mm × 0.400 mm × 0.036 mm and an integrated Si mass dimension of about 1.360 mm × 0.940 mm × 0.456 mm produced 160 mV_{pk}, 2.15 μW or 3272 μW cm^{-3} with an optimal resistive load of 6 kΩ from 2g ($g = 9.81$ m s^{-2}) acceleration at its resonant frequency of 461.15 Hz. This device was compared with other demonstrated MEMS power generators.

(Some figures in this article are in colour only in the electronic version)

1. Introduction

There has been increasing interest in the concept of energy harvesting, which is a process of capturing ambient waste energy and converting it into useable electricity. Traditional power sources such as batteries have limitations in current wireless remote sensor systems, among them are large volume, limited lifetime, environmental pollution and large maintenance requirements. Furthermore, the increasing demands upon mobile devices such as wireless sensor networks and the recent advent of the extremely low power electrical and mechanical devices such as microelectromechanical systems (MEMS) make such renewable power sources very attractive.

A variety of ambient sources such as light, heat and mechanical vibration have been studied as an additional energy supplier. Among these, solar lighting has the highest output power density, but mechanical vibration has been demonstrated to offer great potential where there is an insufficient light source [1]. The three types of electromechanical transducers including electrostatic, electromagnetic and piezoelectric have been utilized to design and build vibration-based energy harvesting devices [2–5]. Piezoelectric energy harvesting devices have been more intensively studied because of their simple configuration, high conversion efficiency and ability for precision control of the mechanical response [5–14].

Most current research on piezoelectric energy harvesting devices is concentrated on bulk prototypes; however, a few groups have demonstrated MEMS devices capable of generating useful power. Marzencki *et al* successfully fabricated a thin film AlN cantilever generator that can generate 0.038 μW from a 0.5g ($g = 9.81$ m s^{-2}) vibration at its resonant frequency of 204 Hz [12]. The output power of their device is limited to low power levels by the properties of AlN. Through FEM simulation, they estimated that higher power could be obtained from a thin film PZT generator due to a much higher piezoelectric constant. Recently, Marzencki

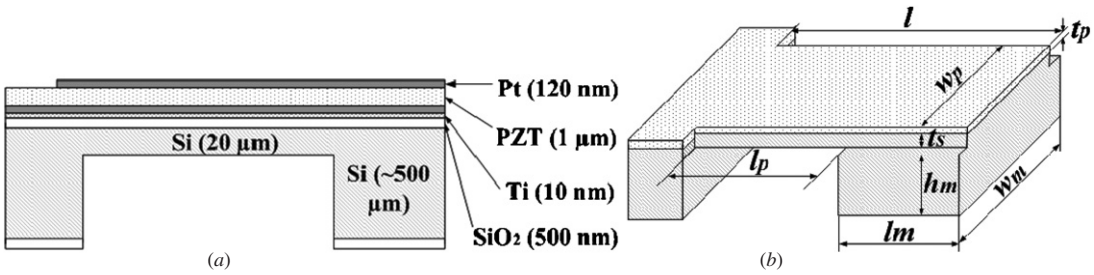

Figure 1. Schematics of (*a*) the side view and thicknesses of a piezoelectric energy harvesting cantilever and (*b*) the simplified two-layer model used for calculation and notations (not to scale).

et al improved upon the power generation capabilities of their devices with a thin film AlN cantilever that can generate 1.97 μW from a 4.0g vibration at its resonant frequency of 1368 Hz [13]. Jeon *et al* developed a d_{33} mode thin film PZT power generating device with interdigitated electrodes that can generate 1.0 μW from a 10.8g vibration at its resonant frequency of 13.9 kHz [9]. Fang *et al* fabricated a MEMS-based PZT cantilever power generator with a nonintegrated Ni proof mass that can generate 2.16 μW from a 1g vibration at its resonant frequency of 609 Hz [8]. While their demonstrated power density is quite high, the proof mass was not integrated with the cantilever which will be an additional difficulty in production. Renaud *et al* fabricated a MEMS PZT cantilever with an integrated proof mass that can generate 40 μW from a mechanical input driving the generator at its resonant frequency of 1.8 kHz and amplitude of 180 nm [14].

While the surveyed devices demonstrate relatively large power generation capabilities, the high resonance frequencies necessary to obtain the power limit the scope of application for these devices. It has been reported that common environmental vibrations such as those found in a building exhibit moderate amplitudes ($<1g$), and lower frequencies, typically between 60 Hz and 200 Hz [5], and the requirements on continuous power for a typical bio-MEMS chip are 10 mW, and 2.8 μW for an intermittent application (once per hour) [15]. This paper presents a PZT energy harvesting cantilever device with an integrated Si proof mass for low frequency (hundreds of hertz) and high amplitude ($>1g$) vibration applications. The design, fabrication and characterization of the device are systematically elaborated.

2. PZT energy harvesting cantilever design

The targeted application environment, that is, the vibration frequency and the acceleration amplitude must be known before designing a resonating piezoelectric energy harvester since maximum output power density is obtained when the vibration frequency matches the resonant frequency of the piezoelectric resonator. It has been reported that the power output will be dramatically reduced when the driving vibration frequency deviates from the resonant frequency [16]. The vibration acceleration level is also important because a device must be able to withstand large vibration amplitudes that can arise in severe environments. Common environmental vibrations exhibit moderate amplitudes ($<1g$), and lower frequencies (60–200 Hz) [5]. The components in an automotive vehicle, however, often experience much higher vibration amplitudes. The ambient environment that we targeted in this effort is one of approximately 140 Hz and above 1g acceleration. These conditions favor a cantilever structure with a proof mass not only since it is much easier to realize a low resonance frequency but also because the cantilever is effective at generating large strains for a given input force compared to other structures.

The MEMS piezoelectric cantilever energy harvesting device in this research consists of a multi-layer structure, as shown in figure 1(*a*). Pt/PZT/Pt/Ti/SiO_2 multilayered films were deposited on a Si substrate. Si was used as the proof mass at the tip to decrease the resonant frequency and to provide a supporting layer under the beam to improve its mechanical strength; SiO_2 was used to compensate the internal stress and insulator between the electrode and Si; interlayer titanium was used to improve the adhesion between PZT and Pt; and Pt was used as the electrodes.

The dimensions of the device were based primarily on the resonant frequency determination. The thickness of the proof mass was limited by the thickness of the 100 mm (4 inch) wafer, approximately 500 μm. In addition, the thickness of the PZT film and the thickness of the Si supporting layer were fixed at 1 μm and 20 μm, respectively. All other thinner layers were ignored to simplify the calculation during the design. A schematic of the simplified model and correlated notations on dimensions used for the calculation is shown in figure 1(*b*).

The resonant frequency of a cantilever (clamped-free structure) without a proof mass can be expressed in terms of the flexural rigidity EI [17] by

$$f_n = \frac{\upsilon_n^2}{2\pi}\frac{1}{l^2}\sqrt{\frac{EI}{m'}} \tag{1}$$

or in terms of the bending modulus per unit width D_p ($D_p = EI/w$) [18, 19] by

$$f_n = \frac{\upsilon_n^2}{2\pi}\frac{1}{l^2}\sqrt{\frac{D_p}{m}} \tag{2}$$

where f_n is the nth mode resonant frequency, υ_n the nth mode eigenvalue, l the length of the cantilever, E the modulus of elasticity, I the area moment of inertia about the neutral axis, m' the mass per unit length of the cantilever beam and w is the

width of the cantilever. For a unimorph laminated composite cantilever, D_p is a function of the Young's moduli of the two materials, E_p (PZT) and E_s (Si), and their thicknesses, t_p and t_s where

$$D_p = \left[E_p^2 t_p^4 + E_s^2 t_s^4 + 2E_p E_s t_p t_s \left(2t_p^2 + 2t_s^2 + 3t_p t_s\right)\right] \times [12(E_p t_p + E_s t_s)]^{-1} \quad (3)$$

and the mass per unit area m is calculated from the thicknesses and densities, ρ_p and ρ_s, of the two materials by

$$m = \rho_p t_p + \rho_s t_s. \quad (4)$$

The resonant frequency of a cantilever with a point proof mass positioned at the free end tip can be approximated by [18]:

$$f_n' = \frac{v_n'^2}{2\pi}\sqrt{\frac{K}{m_e + \Delta m}} \quad (5)$$

where $v_n'^2 = v_n^2\sqrt{0.236/3}$, the effective mass of the cantilever at the tip $m_e = 0.236mwl$, Δm the mass of the point proof mass added to the free end tip and K is the effective spring constant at the tip of the cantilever given by

$$K = \frac{3D_p w}{l^3}. \quad (6)$$

However, when the proof mass is distributed across an area rather than through a point at the end tip it can be treated as a concentrated point load directed through its center of mass. For a distributed proof mass with uniform density and rectangular symmetry located at the free end tip, the center of mass is at a distance of $l_m/2$ from the end tip. The effective spring constant of the cantilever at this location K' is related to the end tip effective spring constant K by [20]

$$K' = K\left(\frac{l}{l - l_m/2}\right)^3. \quad (7)$$

Substituting K' for K into equation (5), the resonant frequency of a unimorph composite cantilever with a large proof mass located at the free end tip is thus

$$f_n' = \frac{v_n^2}{2\pi}\sqrt{\frac{0.236D_p w}{(l - l_m/2)^3(0.236mwl + \Delta m)}}. \quad (8)$$

The targeted resonant frequency was attained by changing the lengths and widths of the cantilever beam and the dimensions of the proof mass.

3. Fabrication and evaluation

A four-mask process was used to fabricate the PZT cantilever, as shown in figure 2. The fabrication process began with a 100 mm low-cost bare silicon wafer. SiO_2 was grown on both sides of the silicon wafer by a wet O_2 method. Interlayer Ti and electrode Pt were deposited one after another by magnetron sputtering. PZT was deposited layer by layer using the sol–gel method to reach a thickness of 1 μm. The top electrode was patterned by the first mask and obtained by a liftoff process after Pt deposition on a layer of patterned photoresist (PR). The bottom electrode together with the cantilever structure was patterned by the second mask and etched by inductively coupled plasma (ICP) reactive ion etching (RIE) to create a bare window for easy access during wire bonding. The cantilever structure without the bottom electrode was then patterned by the third mask and etched by RIE. The back side proof mass was finally patterned by the fourth mask and the cantilever structure was finally released after back side Si RIE.

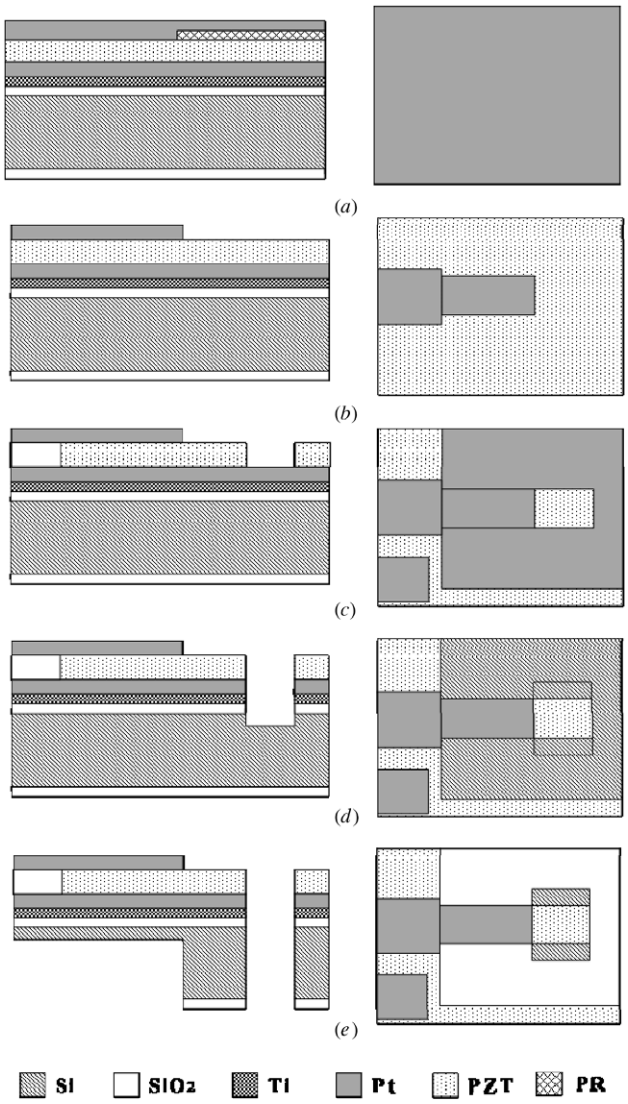

Figure 2. Fabrication flow chart: (*a*) multilayer deposition; (*b*) top electrode patterning by liftoff (mask 1); (*c*) bottom electrode opening via RIE (mask 2); (*d*) cantilever patterning by RIE (mask 3); (*e*) proof mass patterning and cantilever release via backside RIE (mask 4).

The fabricated devices were cleaned, wire bonded and evaluated. The dimensions of one of the devices were measured using SEM (JEOL 7000 FE). The hysteresis loop and the resonant frequency were measured using TF Analyzer 2000 (aixACCT Systems) and impedance analyzer (Agilent Technologies, 4294A). The output behavior was then systematically evaluated using an experimental setup described previously [21].

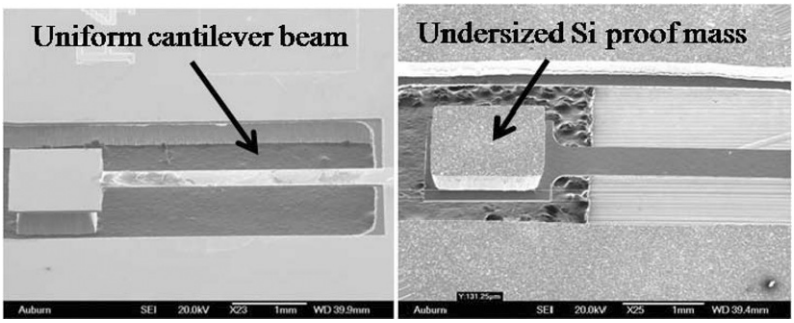

(*a*) (*b*)

Figure 3. SEM pictures of the fabricated PZT cantilever energy harvesting device: (*a*) front side; (*b*) back side.

Table 1. Measured dimensions and effective volume of the PZT device (μm).

l_p	w_p	t_{PZT}	t_{Si}	l_m	w_m	h_m	Volume (mm^3)
3200	400	1	35	1360	940	456	0.6520

4. Results and discussion

4.1. Experimental results

SEM pictures of one of the fabricated cantilever devices are shown in figure 3. From the pictures we can see the clearly defined straight cantilever beam along with the undersized proof mass. The straight beam shows little internal stress, which demonstrates the practicable layer structure of the device and the fabrication process. The undersized proof mass resulted from the shrinkage of the photoresist which was used as a barrier layer during RIE. A thin layer of SiO_2 may be a better choice for the barrier layer even though it would increase the complexity of fabrication.

The measured dimensions of the device and the calculated effective volume are listed in table 1. Both the width and the length of the cantilever beam were uniform and consistent with the designed dimensions, but the width and the length of the proof mass and the thickness of the supporting Si layer were inconsistent with the design due to the shrinkage of the photoresist and the nonuniform etching rate of the RIE system. The thicker supporting layer and the undersized proof mass will result in a higher resonant frequency. However, a SOI (silicon-on-insulator) wafer is a good choice to precisely control the thickness and uniformity of the supporting Si layer.

Figure 4 shows the measured polarization versus the electric field hysteresis loop of the PZT cantilever device after wire bonding. The maximum polarization was 41.3 μC cm^{-2} at an electric field of 25 MV m^{-1}. This value is the same as the value measured before wire bonding. The PZT film retained excellent properties after the long-term fabrication process.

Figure 5 shows the measured resonant frequency of the PZT cantilever using the impedance analyzer. The peak of the phase angle curve is at 462.5 Hz. The calculated value using the measured dimensions is about 423 Hz, a difference of about 9.4%. This discrepancy is attributed mainly to the simplifications to the model ignoring other thinner layers

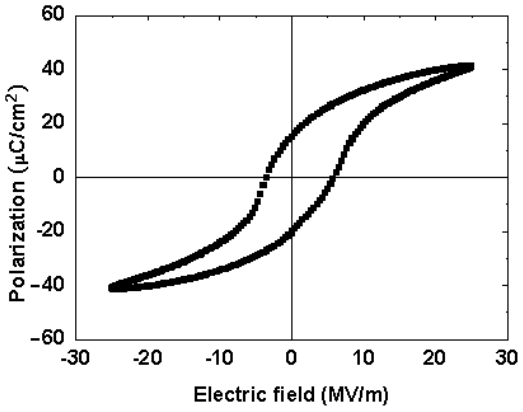

Figure 4. Piezoelectric hysteresis loop measured from the wire-bonded PZT cantilever device.

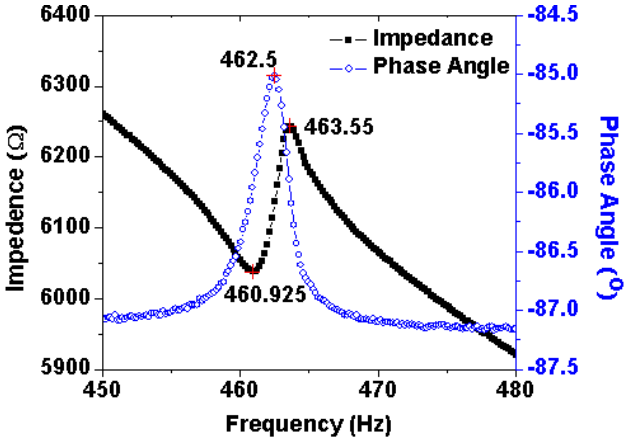

Figure 5. Measured resonant frequency of the PZT cantilever device.

and assuming perfect adhesion between layers, the effect of the large proof mass on the cantilever stiffness through a point away from the end tip and the measurement errors of the physical dimensions of the cantilever, especially on the thickness, which is critical to the resonant frequency. Furthermore, the undersized proof mass and the thicker supporting Si layer resulted in a higher resonant frequency than the target design resonant frequency (140 Hz). To reach the targeted resonant frequency, precise dimension control on

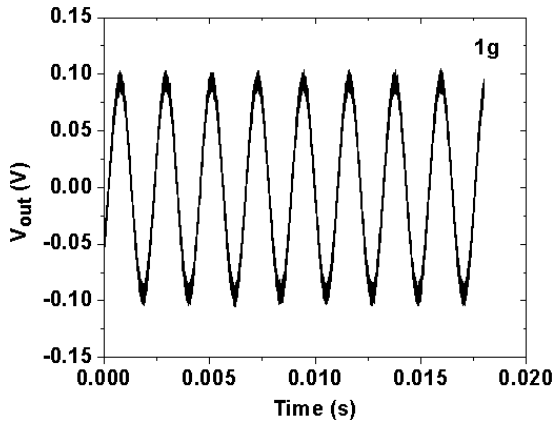

Figure 6. AC output at 1g vibration with a 6 kΩ resistive load.

the process is crucial. Improved fabrication procedures would minimize the difference between the designed and measured resonant frequencies.

The Q-factor calculated from the phase angle peak is about 233. A high Q-factor means low energy loss, which is good for an energy converter; however, a high Q-factor also means large sensitivity of the output behavior of a device to the environmental vibration frequency. A little deviation of the vibration frequency from the device's resonant frequency will induce tremendous reduction of the output power. A lower Q-factor will be preferred as long as the output power is high enough to support the application requirements.

Figure 6 shows the ac output of the device in its optimal resistive load of 6 kΩ from 1g acceleration at its resonant frequency of 461.25 Hz.

Figure 7 shows the peak voltage ($V_{pk} = V_{pk-pk}/2$) and average power $\left(P_{ave} = V_{rms}^2/R_{load}\right)$ of the device versus the resistive load at 0.5g, 1.0g, 1.5g and 2.0g accelerations and corresponding resonant frequencies, which were obtained from the experiment. The resonant frequency gradually decreases with the acceleration amplitude is mainly attributed to the increasing elastic compliance of PZT due to nonlinear effects under large stress [22–24]. The optimal resistive load was found from figure 7(b), which is the resistance when the maximum power generation is obtained. The optimal resistance increases slightly with the excitation acceleration amplitude since the mechanical damping of the device increases with stress [23], and the electrical damping must be increased to match the mechanical damping to maximize the output power. Increasing the resistive load is a convenient approach to increasing the electrical damping because the electrical damping is proportional to the resistive load [25].

The maximum output power of 2.15 μW was obtained at 2g acceleration with a 6 kΩ resistive load resulting in a maximum power density of 3272 μW cm^{-3}. The power density was calculated using the average power divided by the effective volume of the device, which is the volume of the entire beam and the Si proof mass calculated from the measured data in table 1. The effective volume instead of the operation volume was used for comparison with other power generators in references.

The continuous power requirements for a typical bio-MEMS system have been reported to be 10 mW, however; many bio systems may operate with an intermittent power source rather than a continuous one [15]. If an application needs 10 mW of power only once per 80 min, for example, the power generated by this PZT cantilever would be sufficient.

Figure 8 shows the peak voltage and average power of the device versus the vibration frequency at 0.5g, 1.0g, 1.5g and 2.0g accelerations and the corresponding optimal resistive loads obtained from figure 7(b). The resonant frequencies of this device at different accelerations apparently shifted to lower frequency with increasing exciting vibration amplitude. In figure 8(a), the V_{pk} is not linearly related to the acceleration amplitude, but increases more and more slowly. This is because of the nonlinear response of PZT under large stress; both the elastic compliance and damping coefficient increase when the stress is sufficiently large while the piezoelectric constant decreases with increasing stress [24]. The power does not increase in a quadratic relationship with the acceleration but increases more and more slowly for the same reason.

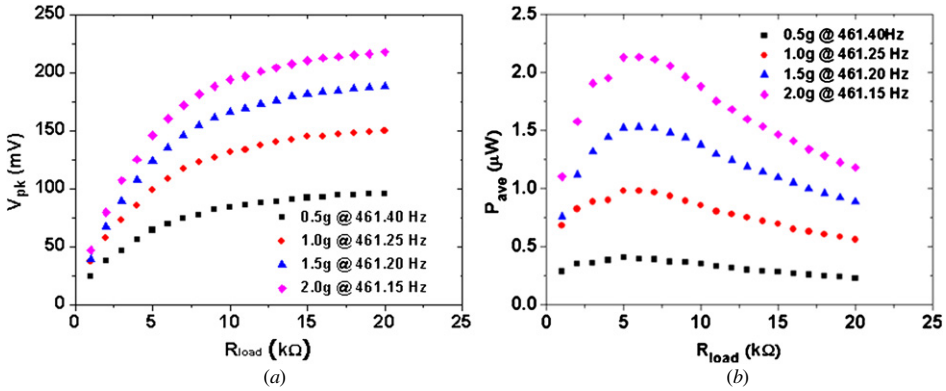

(*a*) (*b*)

Figure 7. (*a*) Peak voltage and (*b*) average power versus resistive load.

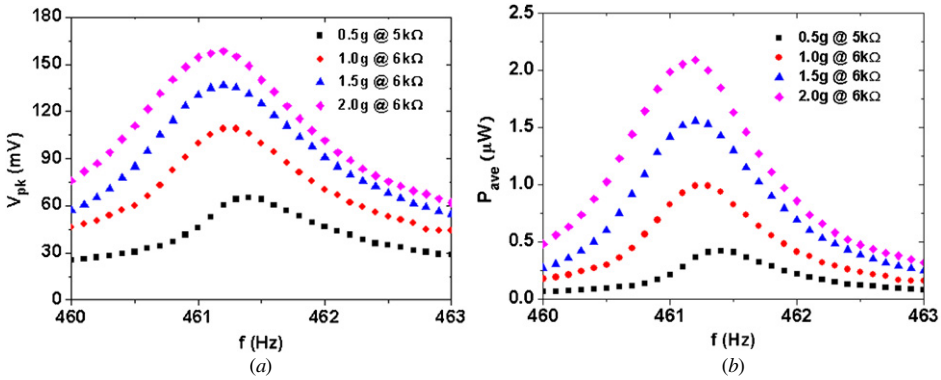

Figure 8. (*a*) Peak–peak voltage and (*b*) average power versus vibration frequency.

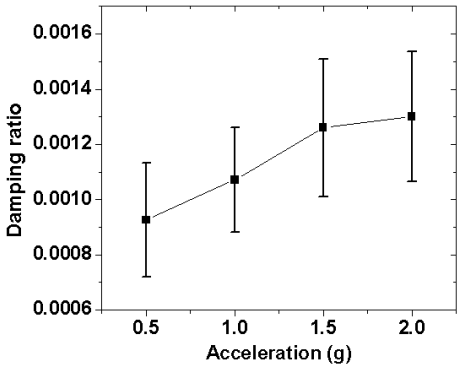

Figure 9. Damping ratio increases with acceleration amplitude.

Besides the output behavior of this device, the damping ratio (ζ) was also calculated at different accelerations. For a damped harmonic oscillator, the mass m, natural angular frequency ω_0, viscous damping coefficient c and the damping ratio ζ (defined as the ratio between the damping coefficient c and the critical damping coefficient c_c) are related by $c = 2m\zeta\omega_0$ [25]. A large damping ratio indicates low-power conversion efficiency and increased energy loss. The ac outputs of the PZT cantilever were recorded separately immediately after stopping the exciting vibration. The damping ratio can be calculated by [25]:

$$\zeta = \frac{1}{2\pi n} \ln(x_1/x_2) \tag{9}$$

where x_1 is the amplitude at one point in time and x_2 is a later amplitude measured after n periods of the sinusoidal response. For each acceleration evaluated, ten segments of the damped waveforms were randomly selected to obtain the amplitudes to be used in calculating the average damping ratios and the results shown in figure 9. The ratio increases with the acceleration due to nonlinearity of PZT under large stress [23].

4.2. Comparison with other published MEMS energy harvesting devices

The working conditions, output behaviors and pictures of this integrated MEMS PZT energy harvesting device together with other published MEMS piezoelectric power generators are listed in table 2 for comparison.

5. Conclusions

A MEMS PZT energy harvesting cantilever with an integrated Si proof mass was designed, fabricated and evaluated. The fabricated device has beam dimensions of about 4.800 mm × 0.400 mm × 0.036 mm with an integrated Si proof mass with dimension of about 1.360 mm × 0.940 mm × 0.456 mm. The effective volume, beam plus proof mass, is about 0.6520 mm^3. It produced 160 mV_{pk}, 2.15 μW or 3272 $\mu W\ cm^{-3}$ with an optimal resistive load of 6 kΩ from 2g acceleration at its resonant frequency of 461.15 Hz.

Acknowledgments

This work is sponsored by a research grant from Industry, the National Science Foundation (NSF-DMR-0605270), and USDA-CSREES (2006-34394-16953).

Table 2. Comparison among MEMS piezoelectric energy harvesting devices.

Author	Device	Effective volume (mm^3)	Power (μW)	Power density ($\mu W\ cm^{-3}$)	A (g)	f (Hz)
Marzencki *et al* [12]	d_{31} AlN cantilever	3.8[a]	0.038	10	0.5	204
Jeon *et al* [9]	d_{33} PZT cantilever	0.027[a]	1.01	37 037[a]	10.8	13.9k
Fang *et al* [8]	d_{31} PZT cantilever	0.1992[a]	2.16	10 843[a]	1.0	608
Marzencki *et al* [13]	d_{31} AlN cantilever	>0.552 [a]	1.97	<3569[a]	4.0	1368
Renaud *et al* [14]	d_{31} PZT cantilever	1.845[a]	40	21 680[a]	1.9[a]	1.8k
Shen *et al* (in this research)	d_{31} PZT cantilever	0.6520	2.15	3272	2.0	462.5

[a] Estimated from data in reference.

References

[1] Beeby S P, Tudor M J and White N M 2006 Energy harvesting vibration sources for microsystems applications *Meas. Sci. Technol.* **17** 175–95

[2] Mitcheson P D, Green T C, Yeatman E M and Holmes A S 2004 Architectures for vibration-driven micropower generators *J. Microelectromech. Syst.* **13** 429–40

[3] Torah R N, Beeby S P, Tudor M J, O'Donnell T and Roy S 2006 Development of a cantilever beam generator employing vibration energy harvesting *PowerMEMS—The 6th Int. Workshop on Micro and Nanotechnology for Power Generation and Energy Conversion Applications (Berkeley)* pp 181–4

[4] Miyazaki M, Tanaka H, Ono G, Nagano T, Ohkubo N, Kawahara T and Yano K 2003 Electric-energy generation using variable-capacitive resonator for power-free LSI: efficiency analysis and fundamental experiment *Proc. Int. Symp. on Low Power Design (Seoul, South Korea Association for Computing Machinery)* pp 193–8

[5] Roundy S, Wright P K and Rabaey J 2003 A study of low level vibrations as a power source for wireless sensor nodes *Comput. Commun.* **26** 1131–44

[6] Kim H W, Batra A, Priya S, Uchino K, Markley D, Newnham R E and Hofmann H F 2004 Energy harvesting using a piezoelectric 'cymbal' transducer in dynamic environment *Japan. J. Appl. Phys.* Part 1 **43** 6178–83

[7] Sodano H A, Lloyd J and Inman D J 2006 An experimental comparison between several active composite actuators for power generation *Smart Mater. Struct.* **15** 1211–6

[8] Fang H B, Liu J Q, Xu Z Y, Dong L, Wang L, Chen D, Cai B C and Liu Y 2006 Fabrication and performance of MEMS-based piezoelectric power generator for vibration energy harvesting *Microelectron. J.* **37** 1280–4

[9] Jeon Y B, Sood R, Jeong J H and Kim S G 2005 MEMS power generator with transverse mode thin film PZT *Sensors Actuators* A **122** 16–22

[10] Priya S, Chen C T, Fye D and Zahnd J 2005 Piezoelectric windmill: a novel solution to remote sensing *Japan. J. Appl. Phys.* Part 2 **44** 104–7

[11] Glynne-Jones P, Beeby S P and White N M 2001 Towards a piezoelectric vibration-powered microgenerator *IEE Proc.* **148** 68–72

[12] Marzencki M, Charlot B, Basrour S, Colin M and Valbin L 2005 Design and fabrication of piezoelectric micro power generators for autonomous microsystems *DTIP7 '05—Symp. on Design Testing Integration and Packaging of MEMS/MOEMS (Montreux, Switzerland)* pp 299–302

[13] Marzencki M, Ammar Y and Basrour S 2007 Integrated power harvesting system including a MEMS generator and a power management circuit *Proc. Int. Conf. on Solid-State Sensors, Actuators and Microsystems (Lyon, France)* pp 887–90

[14] Renaud M, Sterken T, Schmitz A, Fiorini P, Van Hoof C and Puers R 2007 Piezoelectric harvesters and MEMS technology: fabrication, modeling and measurements *Proc. Int. Conf. on Solid-State Sensors, Actuators and Microsystems (Lyon, France)* pp 891–4

[15] Ramsay M J and Clark W W 2001 Piezoelectric energy harvesting for bio MEMS applications *Proc. SPIE—Int. Soc. Opt. Eng.* **4332** 429–38

[16] Roundy S, Leland E S, Baker J, Carleton E, Reilly E, Lai E, Otis B, Rabaey J M, Wright P K and Sundararajan V 2005 Improving power output for vibration-based energy scavengers *IEEE Pervasive Comput.* **4** 28–36

[17] Blevins R D 2001 *Formulas for Natural Frequency and Mode Shape* (Malabar, FL: Krieger Publishing Company) p 158

[18] Yi J W, Shih W Y and Shih W-H 2002 Effect of length, width, and mode on the mass detection sensitivity of piezoelectric unimorph cantilevers *J. Appl. Phys.* **91** 1680–6

[19] Li X, Shih W Y, Aksay I A and Shih W-H 1999 Electromechanical behavior of PZT-brass unimorphs *J. Am. Ceram. Soc.* **82** 1733–40

[20] Sader J E, Larson I, Paul M and White L R 1995 Method for the calibration of atomic force microscope cantilevers *Rev. Sci. Instrum.* **66** 3789–98

[21] Shen D, Choe S Y and Kim D J 2007 Analysis of piezoelectric materials for energy harvesting devices under high-*g* vibrations *Japan. J. Appl. Phys.* **46** 6755–60

[22] Wang Q M, Zhang Q, Xu B, Liu R and Cross L E 1999 Nonlinear piezoelectric behavior of ceramic bending mode actuators under strong electric fields *J. Appl. Phys.* **86** 3352–60

[23] Yao L Q, Zhang J G, Lu L and Lai M O 2004 Nonlinear dynamic characteristics of piezoelectric bending actuators under strong applied electric field *J. Microelectromech. Syst.* **13** 645–52

[24] ANSI/IEEE 1987 *IEEE Standard on Piezoelectricity* Std 176-1987

[25] Roundy S J 2003 Energy scavenging for wireless sensor nodes with a focus on vibration to electricity conversion *Dissertation* University of California, Berkeley